A Comparison of Methods for Linear Cell-to-Cell Mapping and Application Example for Fault Detection and Isolation

Sara Mohon[1] and Pierluigi Pisu[2]

[1,2]*Clemson University International Center for Automotive Research, Greenville, South Carolina, 29607, USA*

smohon@clemson.edu
pisup@clemson.edu

ABSTRACT

In this paper, the Generalized Cell Mapping (GCM) method for a linear system is compared with a new stochastic method for novel cell-to-cell mapping. The authors presented the new stochastic method in a previous paper last year. The two methods are compared in an application example of a vehicle alternator. The alternator may experience three faults including belt slippage, a broken diode, or incorrect controller reference voltage. Fault detection and isolation (FDI) is performed using the two cell-to-cell mapping methods. The results show that the new stochastic method is more computationally intensive but yields better isolation results than the GCM method.

1. INTRODUCTION

Besides high performance, the other most important and desirable features of modern technological systems are safety and reliability. Owing to their increasing complexity, technological systems are becoming more and more vulnerable to faults. These faults, if not handled timely and properly, may lead to severe failures causing damage to property or even human lives. This is particularly true for the complex dynamic systems made of interconnected components where one faulty component can lead to malfunction of the overall system. Therefore, detection and isolation of the faults is of extreme importance in modern technological systems. Early detection and proper handling of faults essentially improve the dependability of the dynamic system ensuring safe operation.

An important tool for analyzing dynamic systems is cell-to-cell mapping as described by Hsu (1980). The dynamic state space of the system is quantized into cells that the system may occupy as time evolves. State variables are considered in intervals instead of a continuum of points. Such a system is justified due to the inherent inaccuracy of physical measurements. Using this framework, the

probability of cell transitions can be computed using various approaches such as Monte Carlo and GCM methods.

In the Monte Carlo method, repeated random samplings and deterministic computations are used to find possible outcomes and their associated probabilities (Kastner, 2010). Using this information, a state probability transition matrix for the system can be constructed (Wang, 1999). The more samplings performed, the more accurate the probability transition matrix (Sobol, 1994).

In the GCM method, the boundaries of image cells are important in determining state transition probabilities (Hsu 1981). The image cell of the current cell are found first. Then the boundaries of the image cell are mapped back to locations on the current cell and when linearly connected form an area within the current cell. Now this area is known to transition to a particular image cell area. The probability associated with this transition is calculated given the total area of the current cell.

The main motivation for formulating the GCM method was to analyze global dynamics of a system (Hsu, 1982). The purpose of the method was to find equilibrium states and periodic motions in the system that can be identified after many mapping steps are performed (Hsu & Chiu 1986). This global analysis can yield a stationary probability transition matrix that does not change with time. Stationary transition matrices allow the global behavior of the system to be analyzed through Markov Chain theory where the entire evolution of cell mapping over time is determined by the stationary transition matrix (Hsu & Guttalu, 1980).

The Monte Carlo and GCM method each rely on repetitive simulations during each time step to calculate transition probabilities. Each method effectively uses information about the initial cell and image cell(s). The amount of computation involved could overwhelm a microcomputer trying to calculate transition probabilities in real-time. These methods are most suitable for offline approaches. Therefore, a new method that only uses information about the initial cell would be a beneficial step toward real-time applications.

The Monte Carlo and GCM approaches can also be computationally burdensome with respect to high dimensional nonlinear systems. Performing the Monte Carlo method on these systems requires huge sampling populations. The GCM method also requires many calculations in order to find image cell boundaries for a nonlinear system. Then all these image cell points must be inversely mapped into the original cell. The feasibility of these methods with nonlinear systems is severely limited.

The new stochastic method proposed by the authors uses the system vector field to calculate state transition probabilities as time evolves without computing image cells. In this paper, the new method will be called the flow method. The flow in/out of a cell through its perimeter is analyzed similar to Green's theorem. The total flow through a cell is comprised of summation of the flow through the sides of the cell. This flow directly impacts the probability of state transition. At each time step, the flow through each side of current state is calculated and then normalized to total flow through whole state perimeter. A time-varying probability transition matrix can be created from these calculations.

Once armed with the above methods for obtaining the probability transition matrices, they can be applied to FDI problems. For example, if an expected state transition has a very low probability, and then the state transitions to this state and possibly continues to transition to low probability states, then this could indicate a fault in the system. This paper applies and compares the GCM and flow methods for fault detection in an alternator system previously described by Mohon and Pisu (2013). Results show that the GCM method yields faster detection time with incomplete isolation of faults. On the other hand, the new stochastic method results in slower detection time and complete isolation at the cost of more computational complexity.

The first section of this paper describes the GCM method. The second section describes the flow method. The third section applies the two methods to an application example with a faulty automotive alternator and compares FDI results. Lastly, some concluding remarks about the usefulness of each method is provided.

2. GENERALIZED CELL MAPPING METHOD

The method for generalized cell mapping is described by C. Hsu in his book (Hsu 1987). Unlike simple cell mapping, where one cell is mapped into a single image cell, generalized cell mapping allows one cell to be mapped to several image cells. Each image cells represents a fraction of the total probability.

Consider the following simple example. Suppose we have a system described by Eq 1. There are two states z1 and z2 and only z2 is observable in output. We can illustrate the state space divided into quantized states 1 through 7 in

Figure **1**. We will also assume some maximum and minimum values for z1.

$$
\begin{bmatrix} \dot{z}_1 \\ \dot{z}_2 \end{bmatrix} = \begin{bmatrix} a_{11} & a_{12} \\ a_{21} & a_{22} \end{bmatrix} \begin{bmatrix} z_1 \\ z_2 \end{bmatrix}
$$
$$
+ \begin{bmatrix} b_{11} & b_{12} & b_{13} \\ b_{21} & b_{22} & b_{23} \end{bmatrix} \begin{bmatrix} u_1 \\ u_2 \\ u_3 \end{bmatrix} \quad (1)
$$
$$
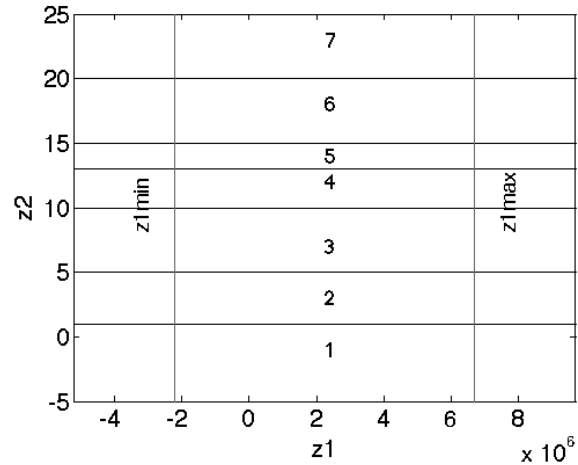y = \begin{bmatrix} 0 & 1 \end{bmatrix} \begin{bmatrix} z_1 \\ z_2 \end{bmatrix}
$$

Figure 1: Quantized states in state space example

Obtaining the image cell boundaries can be thought of as a Monte Carlo exercise. By randomly choosing a large sample of random points within the initial cell (state 4) and applying the dynamic system equations, the new location of the points can be plotted on the 2D state space. Figure **2** and Figure **3** illustrate how the randomly sampled points move in time. A large number of points will clearly delineate the boundary of the new image cell.
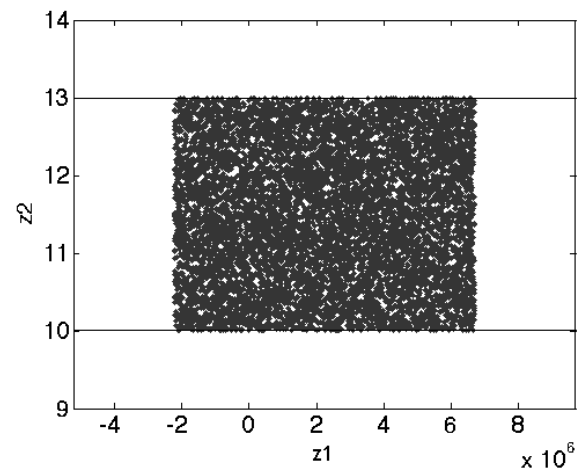

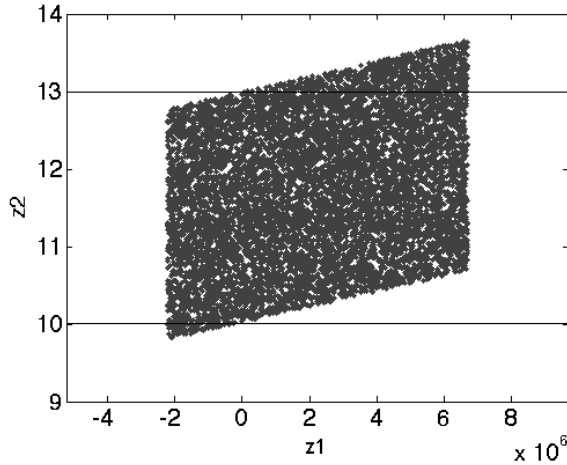Figure 2: Initial cell with randomly sampled points

Figure 3: Image cell containing new position of sampled points after a finite time delta t

The new image cell in this example is clearly a quadrilateral with four vertices. These vertices represent the boundaries of the image cell. Note that the image cell is now spanning states 3, 4, and 5. By using the system dynamic equations, these vertices and other important points can be mapped back into the original cell shown in Figure **4**. This will allow us to determine the regions of the original state that map into other states.
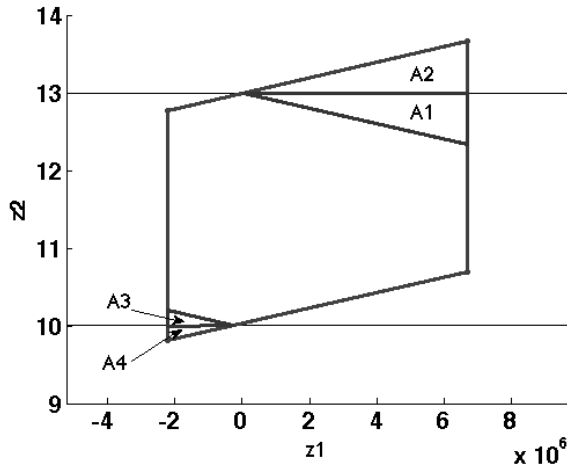

Figure 4: Inverse mapping important points on image cell back into original cell

The regions of the area now defined in the original cell can be used to calculate probabilities of transitioning up or down in the system. Region A2 is mapped back into region A1. Region A4 is mapped back into region A3. The probability to transition up, down, or stay in state 4 is given by the following.

$$P_{up} = A1 \big/ A_{cell}$$
$$P_{down} = A3 \big/ A_{cell} \tag{2}$$
$$P_{stay} = 1 - P_{up} - P_{down}$$

This process can be repeated as the system's state changes along with input values.

3. PROPOSED FLOW METHOD

The flow method was proposed by the authors in a previous paper (2013). This method uses the system's vector field F to determine flow into and out of the current state/cell. The method exploits the divergence theorem and determines the total potential of flow through the cell as the sum of flows through the perimeter of the cell.

A two-dimensional form of the divergence theorem is defined in Eq. (3). We define C as a closed curve, A as the 2D region in the plane enclosed by C, $\bar{n}$ as the outward pointing normal vector of the closed curve C, and $\overline{F}$ as a continuously differentiable vector field in region A. A graph of the 2D divergence theorem for the same 2D system in Eq. 1 is shown in Figure **5**.

$$\iint_A \left(\nabla \cdot \vec{F} \right) dA = \int_C \left(\vec{F} \cdot \vec{n} \right) dr \tag{3}$$
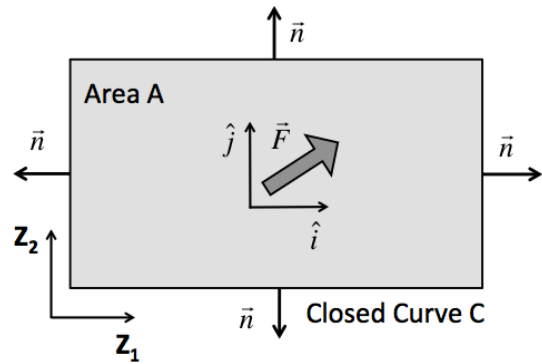

Figure 5. Graph of 2D Divergence Theorem for 2D state space system

We consider that the vector field $\overline{F}$ describes transition flow in and out of the current state along the state boundaries. For the DC electric machine model, $\overline{F}$ is defined as Eq. (4) where $\hat{\imath}$ and $\hat{\jmath}$ are coordinates of vector field F and functions f_1 and f_2 are defined by states z_1 and z_2 from the state space model in Eq. (1).

$$\overline{F} = f_1 \hat{\imath} + f_2 \hat{\jmath}$$
$$\dot{z}_1 = f_1(z_1, z_2, u_1, u_2, u_3) \tag{4}$$
$$\dot{z}_2 = f_2(z_1, z_2, u_1, u_2, u_3)$$

3

The flow through the left and right sides of the area A in Figure **5** will be assumed zero for the alternator system shown in Figure **6**. The line integrals along the state z boundaries will determine flow in and out of the state. The vector field F is illustrated by grey slope field in Figure **6**. Flow out of state z is defined as a positive value φ^+ and flow into state z is a negative value φ^-. Since each side may have flow in and flow out sections, the flow transition point z** or z* is found if necessary and the appropriate limits of integration for flow in and flow out are integrated for each side. Transition points are shown in Figure **6**. Without loss of generality assume $f_2 < 0$ if $z_1 < z^*, z^{**}$ and $f_2 > 0$ if $z_1 > z^*$, z^{**} such that Eq. (5) holds. The upward and downward flow through each side of state z is given by Eq. (6).
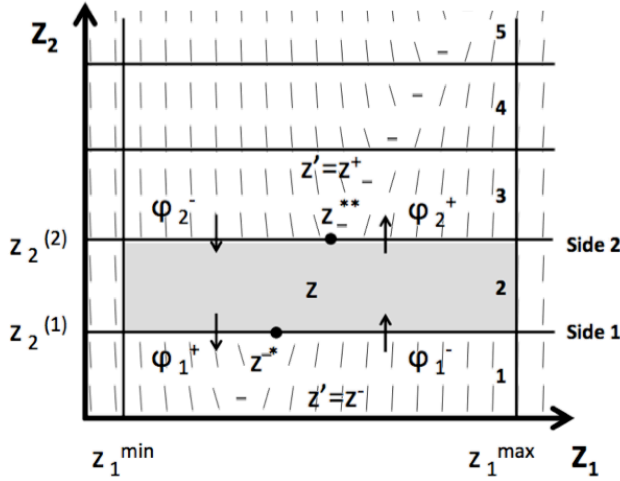

Figure 6. Graph of quantized DC electric machine system with flow definitions

$$f_2(z^*, z_2^{(1)}, u_1, u_2, u_3) = 0$$
$$f_2(z^{**}, z_2^{(2)}, u_1, u_2, u_3) = 0$$
(5)

$$\varphi_1^+ = -\int_{z_1^{min}}^{z_1^*} f_2(z_1, z_2^{(1)}, u_1, u_2, u_3) dz_1 \quad > 0$$

$$\varphi_1^- = -\int_{z_1^*}^{z_1^{max}} f_2(z_1, z_2^{(1)}, u_1, u_2, u_3) dz_1 \quad < 0$$
(6)

$$\varphi_2^- = \int_{z_1^{min}}^{z_1^{**}} f_2(z_1, z_2^{(2)}, u_1, u_2, u_3) dz_1 \quad < 0$$

$$\varphi_2^+ = \int_{z_1^{**}}^{z_1^{max}} f_2(z_1, z_2^{(2)}, u_1, u_2, u_3) dz_1 \quad > 0$$

Next we define φ_{in}, φ_{out}, and φ_{total} in Eq. (7) in order to build probabilities. The sum of the absolute value of all inward flow in defined as φ_{in}. The sum of all outward flow is defined as φ_{out}. The total flow φ_{total} is the sum of φ_{in} and φ_{out}.

$$\varphi_{in} = \left| \varphi_1^- + \varphi_2^- \right|$$
$$\varphi_{out} = \varphi_1^+ + \varphi_2^+$$
(7)
$$\varphi_{total} = \varphi_1^+ + \left| \varphi_1^- \right| + \left| \varphi_2^- \right| + \varphi_2^+$$

The notion of probability can be interpreted as counting types of occurrences and then normalizing the count of each type by the total occurrences. Suppose the occurrences of outward and inward flow defined in Eq. (6) are normalized by the total flow defined in Eq. (7). For example, the probability to transition up will be defined as the outward flow through side 2, φ_2^+, divided by the total flow φ_{total}. We can then define z^+ as the state above current state z and define z^- as the state below current state z. Equation (8) gives the probability to stay within the current state and the probability to transition up or transition down to an adjacent state. Uniform probability distribution is assumed along the borders of each state.

$$1 = \frac{\varphi_{in}}{\varphi_{total}} + \frac{\varphi_{out}}{\varphi_{total}}$$

$$1 = \frac{\left| \varphi_1^- + \varphi_2^- \right|}{\varphi_{total}} + \frac{\varphi_2^+}{\varphi_{total}} + \frac{\varphi_1^+}{\varphi_{total}}$$
(8)

$$1 = \Pr(z' = z \mid z) + \Pr(z' = z^+ \mid z)$$
$$+ \Pr(z' = z^- \mid z)$$

At each time step the probability to stay or transition up or transition down is calculated using the current state boundaries and the current input. This information builds a time-varying probability transition matrix named L that can be constructed as shown in Table 1 for the example of current state z=2 at time t.

Table 1. Example of probability transition matrix L for current state z=2 at a time t

		Future State z'			
		1	2	3	4
Current State z	1	0	0	0	0
	2	$\Pr(z' = z^- \mid z)$	$\Pr(z' = z \mid z)$	$\Pr(z' = z^+ \mid z)$	0
	3	0	0	0	0
	4	0	0	0	0

Thus far, the new method formulation has shown the 2D case. The new method can also be extended for the 3D case using 3D divergence theorem defined in Eq. (3). Define V as a closed volume, A as the surface area of V, $\bar{n}$ as the outward pointing normal vector of the closed volume V, and $\bar{F}$ as a continuously differentiable vector field in volume V. A picture for a cubic volume is shown in Figure **7**.
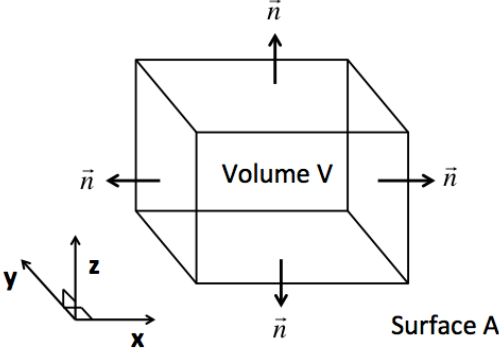
4

$$\iiint_V \left(\nabla \cdot \vec{F}\right)dV = \iint_A \left(\vec{F} \cdot \vec{n}\right)dA \qquad (3)$$

Figure 7. Graph of 3D Divergence Theorem

This method can also be extended to higher dimensions as well using the same procedure.

4. APPLICATION EXAMPLE: EPGS SYSTEM

Today's vehicles require higher electrical demands than ever before due to more mandated safety technology and popular consumer technology integrated within the vehicle. The purpose of the vehicle's electrical power generation storage (EPGS) system is to maintain the necessary electrical power needed to start the vehicle and keep it running smoothly. A healthy EPGS system is crucial for proper operation of a vehicle and have been investigated in previous literature.

Scacchioli, Rizzoni, and Pisu (2006) proposed a fault isolation approach for an EPGS system using two equivalent alternator models. One equivalent model for a healthy alternator and one equivalent model for an alternator with one broken diode. Parity equations and three residuals with constant thresholds were used for fault isolation. The approach assumed a 3000 second Federal Urban Driving Schedule (FUDS) cycle.

Zhang, Uliyar, Farfan-Ramos, Zhang, and Salman (2010) proposed a fault isolation approach for an EPGS system using parity relations trained by Principal Component Analysis (PCA). Three residuals with constant thresholds were used for isolation. The approach assumed a staircase profile for both load current and alternator speed input, which is not a realistic scenario.

Hashemi and Pisu (2011) proposed a fault isolation approach for an EPGS system using two observers and three residuals. The approach assumed a staircase profile for load current and a portion of the FUDS cycle for alternator speed. Adaptive thresholds were used for isolation. In other similar work, Hashemi and Pisu (2011) showed the same approach but created a reduced order adaptive threshold model using Gaussian fit of data. The second approach was less computationally intensive.

Scacchioli, Rizzoni, Salman, Onori, and Zhang (2013) proposed a fault isolation approach for an EPGS system using one equivalent EPGS model that used parity equations to produce three residuals for fault isolation. The approach used a staircase profile for both load current and alternator speed input.

As stated, previous work for fault isolation in an EPGS system has included observers and parity relations. The approaches with observers were built for linear systems that approximate the nonlinear behavior of the EPGS system. These approaches cannot be extended for direct use on the nonlinear system itself. At least three residuals are required for all previous approaches. It is also concerning that some approaches were not validated using real driving situations. Therefore these approaches have limited scopes.

4.1. Model for EPGS System

This paper analyzes the EPGS system shown in Figure **8** as modeled by Scacchioli et al. (2006). It consists of a voltage controller, alternator, and battery. The controller can be an electronic control unit or a voltage controller on the alternator itself. In this paper, the controller is a part of the alternator to regulate field voltage. The alternator model consists of an AC synchronous generator, three phase full bridge diode rectifier, voltage controller, and excitation field.

The engine crankshaft mechanically spins the generator's rotor by use of a belt and pulley. The rotor is a ferrous metal wrapped with a single conductive winding. When the controller applies a small field voltage to the winding, a small field current flows through the winding. The flow of current through the winding produces a magnetic rotor with a north and south pole. However, the stator is composed of three phase stationary windings. As the magnetic rotor moves relative to the conductive stator windings, an electromotive force is induced in the stator windings. If the stator windings are connected to an electrical load, then AC current will flow in each of the three stator windings. The three currents are sent to a diode bridge rectifier to produce DC current for electrical loads or for recharging the battery. Therefore, the alternator takes mechanical energy of the engine and produces electrical energy for the battery or loads of the vehicle.
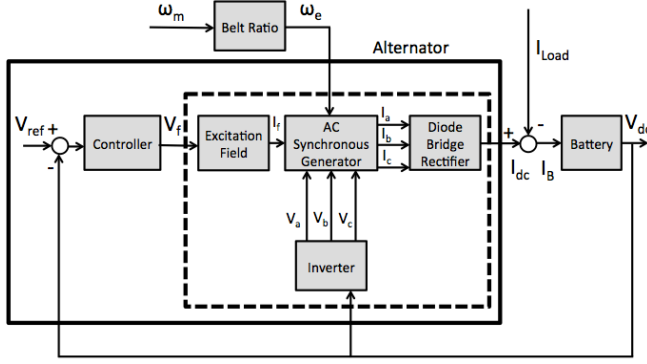
Figure 8. EPGS model

The model for the EPGS system results in a complex nonlinear system but can be more easily modeled by an equivalent DC electric machine as described by Sacchioli et al. (2006). The dashed line in Figure **8** encompasses the components represented by the DC model.

The DC electric machine is modeled by the state space system in Eq. (9) as shown by Hashemi (2011).

$$
\begin{bmatrix} \dot{z}_1 \\ \dot{z}_2 \end{bmatrix} = \begin{bmatrix} 0 & a_{12}(\omega_e) \\ 1 & a_{22}(\omega_e) \end{bmatrix} \begin{bmatrix} z_1 \\ z_2 \end{bmatrix}
$$
$$
+ \begin{bmatrix} b_{11}(\omega_e) & b_{12}(\omega_e) & b_{13}(\omega_e) \\ 0 & b_{22}(\omega_e) & b_{23}(\omega_e) \end{bmatrix} \begin{bmatrix} u_1 \\ u_2 \\ u_3 \end{bmatrix} \quad (9)
$$
$$
y = \begin{bmatrix} 0 & 1 \end{bmatrix} \begin{bmatrix} z_1 \\ z_2 \end{bmatrix}
$$

Equation (9) has two states z_1 and z_2 and inputs u_1, u_2, and u_3. The system inputs represent the alternator field voltage V_f, angular frequency of alternator ω_e, and dc voltage of the battery V_{dc} also shown in Eq. (10). The coefficients a_{12}, a_{22} and $b_{11}\ldots b_{23}$ are functions of engine speed and were found using system identification by Hashemi (2011) using test data at different constant engine speeds. In this model, state z_2 is the measurable quantity I_{dc} which is the rectified output current of the alternator.

$$
\begin{aligned}
y_2 &= I_{dc} = z_2 \\
u_1 &= V_f \\
u_2 &= \omega_e \\
u_3 &= V_{dc}
\end{aligned} \quad (10)
$$

4.2. Possible Faults in EPGS System

The EPGS system is important in every vehicle and faults in the system need to be detected and isolated as quickly as possible to prevent costlier damage. This paper considers three common faults that occur in an EPGS system. Possible fault locations in EPGS system are bolded in Figure **9**.

1. *Voltage controller fault*: This fault occurs when the reference voltage V_{ref} is incorrectly raised or lowered by a percentage of the nominal V_{ref}. The fault can cause the alternator to overcharge or undercharge the battery.

2. *Open diode rectifier fault*. This fault occurs when a diode in the diode bridge rectifier breaks. The fault results in a large ripple in battery voltage V_{dc} and alternator output current I_{dc} thereby decreasing the efficiency of alternator output.

3. *Belt slip fault*. This input fault occurs when the belt between the engine crankshaft and alternator pulley slips due to insufficient tension. The belt slip causes a decrease in alternator rotational speed ω_e and a decrease in alternator output voltage. To compensate, the voltage controller increases the field voltage and/or the battery must discharge more often to meet load demand. This can age the battery prematurely. Belt slip can signify the belt is worn and needs to be replaced.
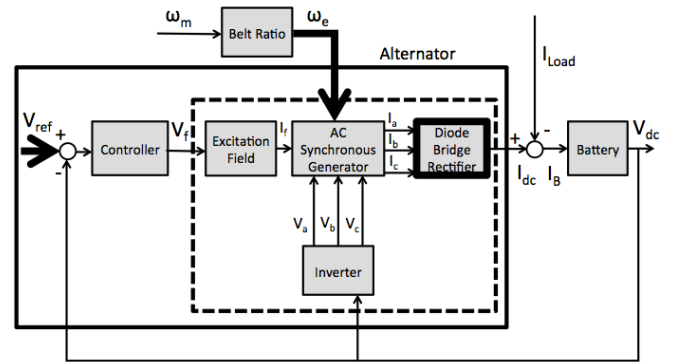

Figure 9: Possible faults in EPGS model

4.3. Simulation Results

Previous work by Scacchioli et al. (2006) yielded a complete nonlinear EPGS model. This nonlinear model uses ω_e, I_{load}, and V_{ref} as inputs and yields V_f, V_{dc}, and battery dc current I_{dc} as output. Diagnostics for the belt fault case, diode fault case, and voltage controller fault case are accomplished by using the flow model and GCM model. The flow model procedure is illustrated in Figure **10** and the GCM model procedure is illustrated in Figure **11**.
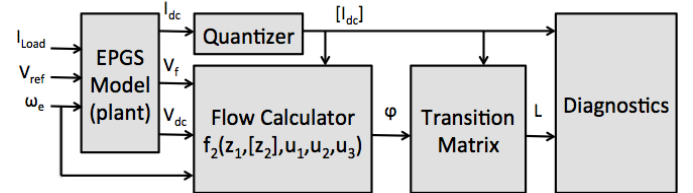

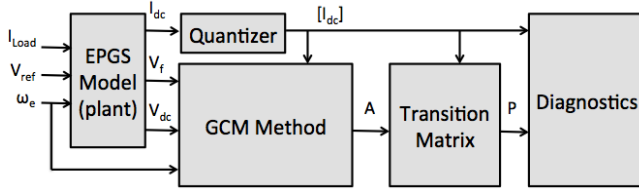Figure 10. EPGS model with flow method

Figure 11: EPGS model with GCM method

The inputs for the nonlinear EPGS Simulink model are provided in Mohon et al (2013).

Table 2 details the selected injection time and magnitude of fault relative to nominal that were injected during simulation. In other words, the nominal inputs were modified to simulate a fault.

Table 2. Fault injection time and magnitude

Fault	Injection time (s)	Modified Input	Resulting % drop with respect to nominal
Belt Slip	10	ω_e	80
Open Diode	10	V_{dc}	N/A (one broken diode)
Voltage Controller	10	V_{ref}	30

Output z_2 range for nominal and faulty cases must be quantized into rectangles to find the probability transition matrix over time. Output z_2 is quantized into 12 states with names 1-12. The same boundaries and names will be used for faulty cases as well.

The z_1 range for this simulation is z_1^{min} is -2.210e+06 and z_1^{max} is 6.683e+06. Given the z_1 range, the quantized states, and u_1, u_2, and u_3, the probability transition matrix can now be calculated using the f_2 function from Eq. (1).

The probability transition matrix L contains the prediction of the most likely quantized state z' = z_L and its probability P(z' = z_L) at the next time step. The most likely probability and most likely predicted state can be compared with the quantized output state [I_{dc}] that actually occurs. If there is a relatively high probability of a particular state transition occurring and that state transition does not occur, then a fault may be present. An example of predicted state probabilities, predicted states, and output states over time for belt fault case is shown in Figure **12** and Figure **13**.

Disagreement between predicted and output states are clear after calculating the difference of quantized output state [I_{dc}] and the predicted state. This difference is defined as the residual r in Eq. (11). The residual results for each fault case using flow method are shown in Figure **14** through Figure **16**. The residual results for each fault case using GCM method are shown in Figure **17** through Figure **19**.
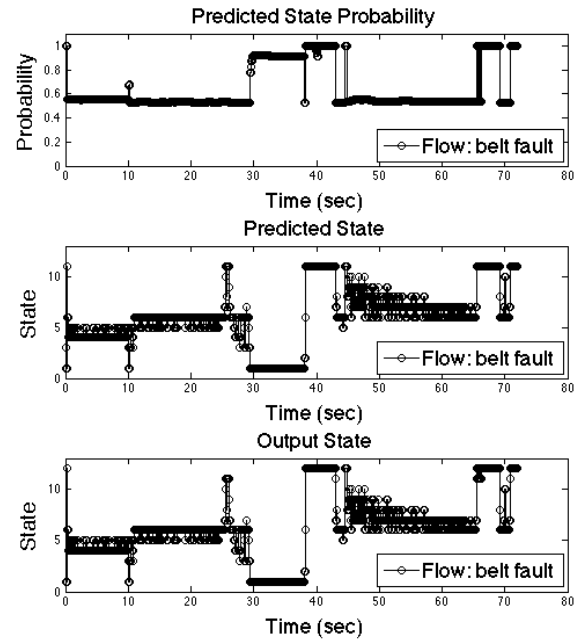

Figure 12. Belt fault outputs for flow method

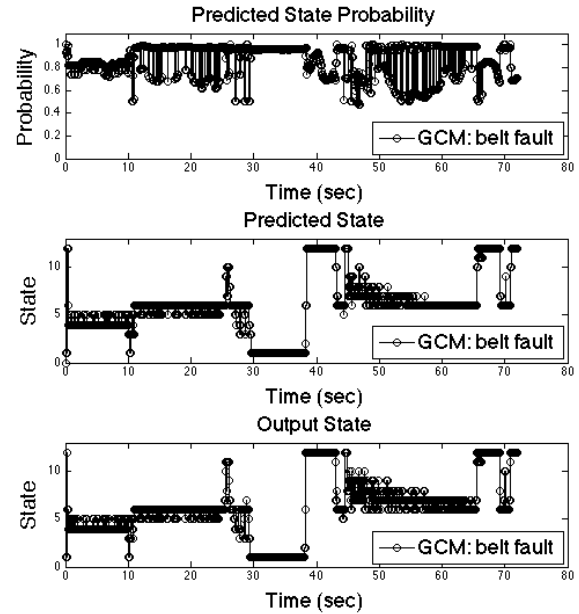Figure 13: Belt fault outputs for GCM method

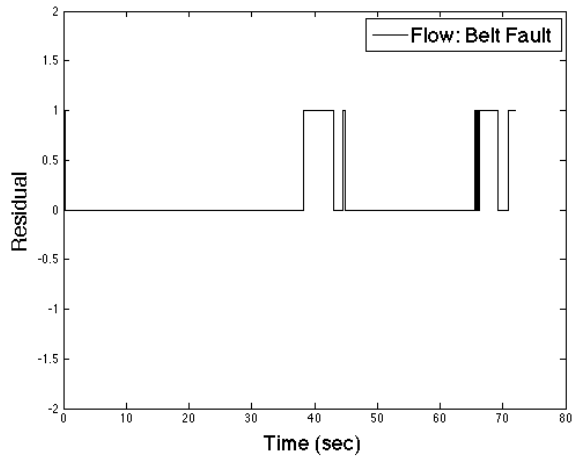$$r = [I_{dc}] - [I_{dc,predicted}] \qquad (11)$$

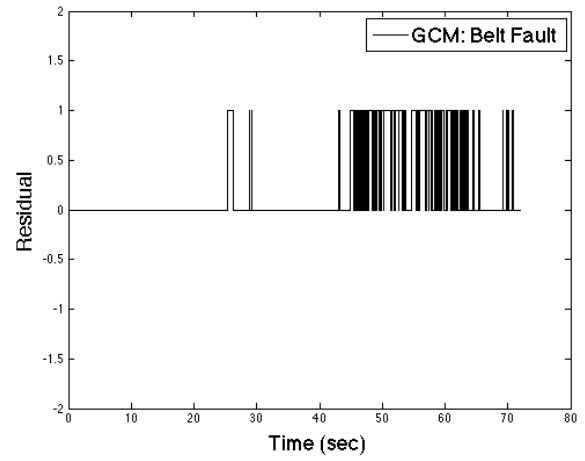Figure 14. Belt fault residual for flow method
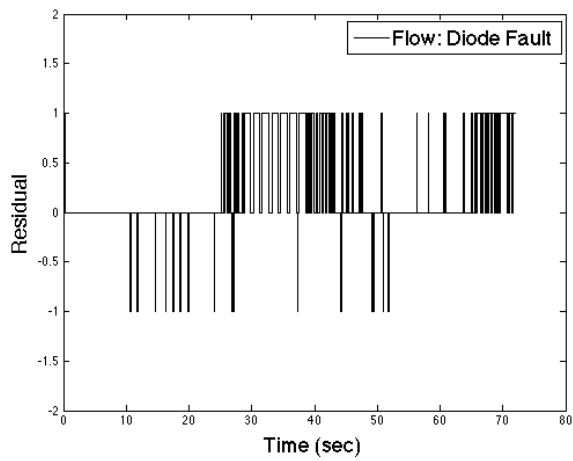

Figure 17: Belt fault residual for GCM method

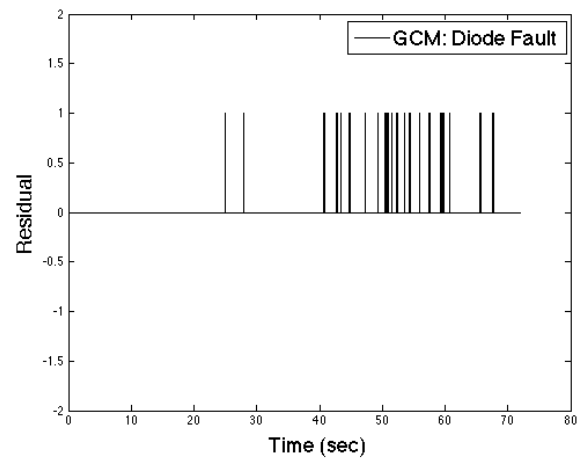Figure 15. Diode fault residual for flow method

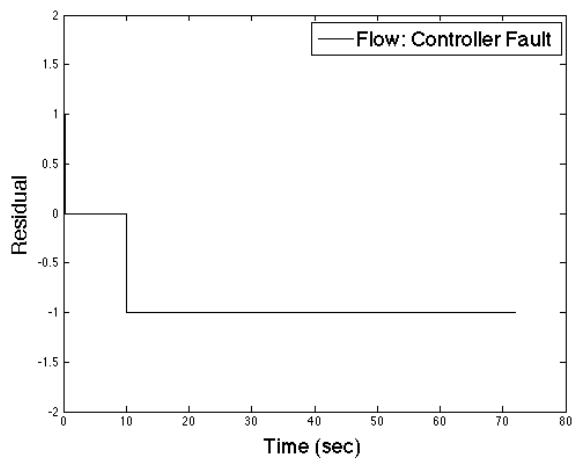Figure 18: Diode fault residual for GCM method

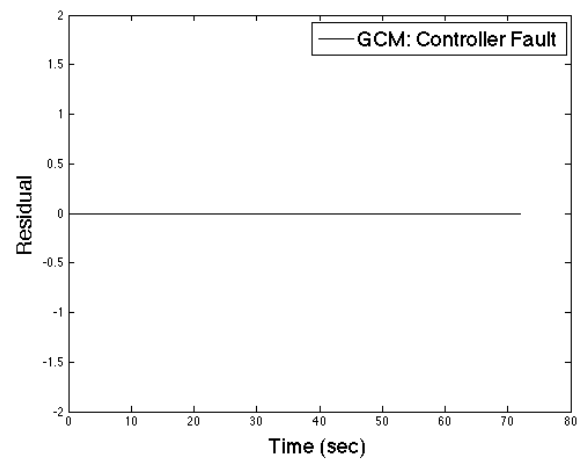Figure 16. Voltage controller fault residual for flow method

Figure 19: Voltage controller fault residual for GCM method

4.3.1. Analysis of Flow Method Results

All three fault cases using the flow method show a short-term disagreement r ≠ 0 between predicted and output states at time t=0.2 seconds but returns to agreement r = 0 immediately at t=0.3 seconds. The disagreement occurs before a fault is injected at time t=10 seconds. This disagreement at t=0.2 could trigger a false alarm during fault detection. Similar rapid switching behavior also occurs in the diode fault residual in Figure 17. To distinguish between the similar switching behavior of false alarms with real faults and to build confidence in the diagnostic algorithm, a fault will only be detected if the residual shows disagreement for at least 0.2 seconds. The belt fault will be detected at t=38.4 seconds. The diode fault will be detected at t=10.7 seconds. The controller fault will be detected at 10.2 seconds.

Isolation of a detected fault will be achieved by monitoring the switching behavior during a finite time window following detection. The belt fault appears in the residual when the load current increases or decreases. Due to the quick duration of load current change, the belt fault is also present for a short time in the residual lasting between two to four seconds. The diode fault causes a large ripple in the alternator output current. This ripple causes frequent and rapid switching behavior from agreement to disagreement in the residual. The controller fault is the only fault case where there is residual disagreement for the entire duration of the fault. Therefore, the mean $\bar{r}$ of the absolute value of the residuals during a finite time window can be used to isolate each fault as defined in Eq. (12). The time window is chosen based on data behavior. For the data in this paper, a six second window was used. Table 3 shows the mean value calculations for each fault using the six second window immediately after fault detection.

$$\bar{r} = \frac{\sum_{i=1}^{n} |r_i|}{n} \qquad (12)$$

Table 3. Mean $\bar{r}$ for six second window using flow method

Fault	Mean $\bar{r}$
Belt Slip	0.75
Open Diode	0.08
Voltage Controller	1

Appropriate constant thresholds for $\bar{r}$ can isolate the fault. For this paper, if $\bar{r}$ is between 0.5 and 1 the fault is due to belt slip. If $\bar{r}$ is 1 the fault is due to the controller. Otherwise, the fault is due to an open diode.

Based on this approach, the belt fault will be isolated at t=44.4 seconds; the diode fault will be isolated at t=16.7 seconds; the controller fault will be isolated at time t=16.3 seconds.

4.3.2. Analysis of GCM Method Results

The GCM method residuals show similar behavior compared to the flow method residuals. For the GCM method, fault detection will occur when the residual shows disagreement for at least 0.2 seconds. The belt fault will be detected at t=10.1 seconds. The diode fault will be detected at t=52.5 seconds. The controller fault will not be detected or isolated because the residual never deviates from zero. The controller fault causes the output to transition to a nonadjacent cell and GCM method allows for nonadjacent cell transitions. Therefore, the residual of controller fault is always zero.

Isolation of the detected fault can be attempted by Eq. (12) with using a six second window immediately after fault detection. Table 5 shows the mean value calculation for each fault. The belt slip fault can be isolated if $\bar{r}$ is between 0.1 and 0.2. The open diode fault can be isolated if $\bar{r}$ is between 0 and 1. However, the voltage controller fault cannot be isolated. The residual never deviates from zero during the entire dataset. Therefore, the voltage controller fault cannot be isolated using GCM method.

Table 4. Mean $\bar{r}$ for six second window using GCM method

Fault	Mean $\bar{r}$
Belt Slip	0.15
Open Diode	0.08
Voltage Controller	0

4.3.3. FDI Summary

Table 5 contains the detection and isolation times for both flow and GCM methods. The flow method can isolate all three faults while the GCM method can isolate only belt slip and open diode faults. The flow method can isolate the open diode fault faster than the GCM method. The GCM method can isolate the belt slip fault faster than the flow method. It is clear that the flow method gives best results since all fault detection and isolation is achievable.

Table 5. Fault injection time and magnitude

	Fault	Belt Slip	Open Diode	Voltage Controller
	Injection time (s)	10	10	10
Flow Method	Detection time (s)	38.4	10.7	10.2
Flow Method	Isolation time (s)	44.4	16.7	16.3
GCM Method	Detection time (s)	25.6	52.5	N/A
GCM Method	Isolation time (s)	31.6	58.5	N/A

Different fault magnitudes might require different isolation thresholds. This paper only considers three discrete fault modes.

5. CONCLUSION

This paper compares the GCM method and a new stochastic method for calculating state transition probabilities within a dynamic system. The methods are compared by detecting and identifying faults in a vehicle alternator system. The methods vary based on computational complexity and the ability to isolate all faults. The GCM method could not detect the controller reference fault but did isolate the belt fault faster than the new stochastic method. Overall, the new stochastic method is preferred since it can complete the FDI analysis even at the cost of computational effort.

NOMENCLATURE

ω_m engine rotational speed
ω_e alternator rotational speed
V_{dc} battery DC voltage
V_f field voltage
V_{ref} voltage controller reference
I_{dc} alternator output current
I_{load} vehicle load current
I_B battery charging current
z_1 first state space state
z_2 second state space state and output
u state space input
$a(\omega_e)$ state space parameter dependent on alternator rotational speed

$b(\omega_e)$ state space parameter dependent on alternator rotational speed
z current state
z' possible future state
z_1^{min} minimum z_1 value
z_1^{max} maximum z_1 value
z^* flow transition point on z_1 axis on side 1 of state z
z^{**} flow transition point on z_1 axis on side 2 of state z
$z_2^{(1)}$ upper boundary of state z
$z_2^{(2)}$ lower boundary of state z
φ^+ flow up
φ^- flow down
f general function
$\bar{F}$ Field vector
$\bar{n}$ normal vector
C general closed curve
A area within curve C
r line integral direction along curve C
φ_{in} total flow into state z
φ_{out} total flow out of state z
φ_{net} net flow for given state z
z^+ state above state z
z^- state below state z
L time varying probability transition matrix
$[I_{dc}]$ quantized alternator output current
r residual
$\bar{r}$ mean of absolute value of residual
n number of data points in residual

REFERENCES

Chiu, H. M. & Hsu, C. S. (1986). A Cell Mapping Method for Nonlinear Deterministic and Stochastic Systems—Part II: Examples of Application. *ASME Journal of Applied Mechanics*. September Vol. 53. pp. 702-710. Doi: 10.1115/1.3171834

Hashemi, A., & Pisu, P. (2011). Adaptive Threshold-based Fault Detection and Isolation for Automotive Electrical Systems (pp. 1013-1018), *World Congress on Intelligent Control and Automation*. June 21-25, Taipei, Taiwan. doi: 10.1109/WCICA.2011.5970668

Hashemi, A., & Pisu, P. (2011). Fault Diagnosis in Automotive Alternator System Utilizing Adaptive Threshold Method. *Annual Conference of Prognostics and Health Management Society*. September 25-29, Montreal, Canada.

Hashemi, A., (2011). *Model-Based System Fault Diagnosis Utilizing Adaptive Threshold with Application to Automotive Electrical Systems*. Masters dissertation. Clemson University, Clemson, South Carolina, USA. http://etd.lib.clemson.edu/documents/1314212419/Hashemi_clemson_0050M_11327.pdf

Hsu, C. S. (1980). A Theory of Cell-to-Cell Mapping Dynamical Systems. *ASME Journal of Applied Mechanics*. December Vol. 47. pp. 931-939. Doi:10.1115/1.3153816

Hsu, C. S. & Guttalu, R. S. (1980). An Unravelling Algorithm for Global Analysis of Dynamical Systems: An Application to Cell-to-Cell Mappings. *ASME Journal of Applied Mechanics*. December Vol. 47. pp. 940-948. Doi: 10.1115/1.3153817

Hsu, C. S. (1981). A Generalized Theory of Cell-to-Cell Mapping for Nonlinear Dynamical Systems. *ASME Journal of Applied Mechanics*. September Vol. 48. pp. 634-642. Doi: 10.1115/1.3157686

Hsu, C. S. (1982). A Probabilistic Theory of Nonlinear Dynamical Systems Based on the Cell State Space Concept. *ASME Journal of Applied Mechanics*. December Vol. 49. pp. 895-902. Doi: 10.1115/1.3162633

Hsu, C. S. & Chiu, H. M. (1986). A Cell Mapping Method for Nonlinear Deterministic and Stochastic Systems— Part I: The Method of Analysis. *ASME Journal of Applied Mechanics*. September Vol. 53. pp. 695-701. Doi: 10.1115/1.3171833

Hsu, C. S., John F., Marsden, J. E., & Sirovich, L. (Eds.). (1987). *Cell-to-Cell Mapping: A Method for Global Analysis for Nonlinear Systems*. New York: Springer.

Kastner, M. (2010). Monte Carlo Methods in Statistical Physics: Mathematical Foundations and Strategies. *Communications in Nonlinear Science and Numerical Simulation*. June Vol. 15. pp. 1589-1602. Doi: 10.1016/j.cnsns.2009.06.011

Mohon, S., & Pisu, P. (2013). A Stochastic Modeling Approach of Quantized Systems with Application to Fault Detection and Isolation of an Automotive Electrical Power Generation Storage System. *Annual Conference of the Prognostics and Health Management Society*, October 14-17, New Orleans, Louisiana.

Scacchioli, A., Rizzoni, G., & Pisu, P., (2006). Model-Based Fault Detection and Isolation in Automotive Electrical Systems, *ASME International Mechanical Engineering Congress and Exposition* (pp. 315-324), November 5-10, Chicago, Illinois, USA. doi: 10.1115/IMECE2006-14504

Sobol, I. (1994). *A Primer for the Monte Carlo Method*. Boca Raton: CRC Press.

Wang, J. (1999). Transition Matrix Monte Carlo Method. *Proceedings of the Europhysics Conference on Computational Physics (CCP)*. September Vol. 121. pp. 22-25. Doi: 10.1016/S0010-4655(99)00270-2

BIOGRAPHIES

Sara Mohon was born in Groton, Connecticut in 1987. She received her B.S. in Physics from the College of William and Mary (Williamsburg, VA, USA) in 2009 and M.S. in Automotive Engineering from Clemson University (Clemson, SC, USA) in 2012. She is currently a Ph.D. student at Clemson University studying Automotive Engineering. She has completed summer internships at NASA Langley Research Center (Hampton, VA, USA) Thomas Jefferson National Accelerator Facility (Newport News, VA, USA), NOAA David Skaggs Research Center (Boulder, CO, USA), and Johns Hopkins University Applied Physics Laboratory (Laurel, MD, USA). She has completed a battery research project at BMW Manufacturing Company (Spartanburg, SC, USA) that resulted in filing a patent about methods to determine the condition of a battery. Her research interests are control, diagnostics, and prognostics for hybrid vehicles and electric vehicles. She is a member of ASME, SAE, SWE, and IEEE and received the national SEMA Top Student Award in 2012.

Pierluigi Pisu was born in Genoa, Italy in 1971. He received his Ph.D. in Electrical Engineering from Ohio State University (Columbus, Ohio, USA) in 2002. In 2004, he was granted two US patents in area of model-based fault detection and isolation. He is currently an Associate Professor in the Department of Automotive Engineering at Clemson University and holds a joint appointment with the Department of Electrical and Computer Engineering at Clemson University. He is also a faculty member at the Clemson University International Center for Automotive Research. His research interests are in the area of fault diagnosis with application to vehicle systems, and energy management control of hybrid electric vehicles; he also worked in the area of sliding mode control and robust control. He is member of the ASME and SAE, and a recipient of the 2000 Outstanding Ph.D. Student Award by the Ohio State University Chapter of the Honor Society of Phi Kappa Phi.